# Evolution of Electrical, Chemical, and Structural Properties of Transparent and Conducting Chemically Derived Graphene Thin Films

By *Cecilia Mattevi,* Goki Eda, Stefano Agnoli, Steve Miller, K. Andre Mkhoyan, Ozgur Celik, Daniel Mastrogiovanni, Gaetano Granozzi, Eric Garfunkel,* and *Manish Chhowalla**

**A detailed description of the electronic properties, chemical state, and structure of uniform single and few-layered graphene oxide (GO) thin films at different stages of reduction is reported. The residual oxygen content and structure of GO are monitored and these chemical and structural characteristics are correlated to electronic properties of the thin films at various stages of reduction. It is found that the electrical characteristics of reduced GO do not approach those of intrinsic graphene obtained by mechanical cleaving because the material remains significantly oxidized. The residual oxygen forms $sp^3$ bonds with carbon atoms in the basal plane such that the carbon $sp^2$ bonding fraction in fully reduced GO is ~0.80. The minority $sp^3$ bonds disrupt the transport of carriers delocalized in the $sp^2$ network, limiting the mobility, and conductivity of reduced GO thin films. Extrapolation of electrical conductivity data as a function of oxygen content reveals that complete removal of oxygen should lead to properties that are comparable to graphene.**

## 1. Introduction

Graphene is a one-atom-thick layer of carbon with remarkable electronic properties that have focused the attention of scientists and engineers. In particular, graphene is a semiconductor with zero band gap and high carrier mobilities and concentrations, and shows nearly ballistic transport at room temperature.[1,2] A challenging aspect of graphene integration into electronic devices is the exfoliation of graphite into individual sheets in a controlled, scalable, and reproducible way. The reliable technique to produce single layer graphene of high quality is the micromechanical cleavage.[3] However, this route is not practical for large-scale integration of graphene. Exfoliation of individual to few layered graphene sheets via agitation in a carefully chosen solvent and maintaining a stable suspension has been recently investigated.[4] However, the reported yield of single-layered graphene was found to be disappointingly small (<1 wt %). Growth of graphene on specific substrates (SiC and on transition metals) has also been demonstrated.[5–7] It is unclear if uniform deposition over large areas can be obtained using these methods and whether the grown graphene can be easily transferred onto more desirable substrates. Recent progress on transfer printing of CVD grown graphene appears to be promising for large area electronics.[8]

The exfoliation of graphite oxide is efficient and results in high yields of single-layered graphene oxide (GO).[9] The individual graphene oxide sheets can then be readily deposited on virtually any substrate over large areas using solution based methods[10] and transfer printing.[11] GO forms over a range of O:C stoichiometries, with the oxygen bound to the carbon in the basal plane in the form of hydroxyl and epoxy functional groups (in variable ratios depending on the synthesis protocol),[12,13] and as carbonyl and carboxyl groups at the sheet edges. These functional groups make graphene oxide sheets strongly hydrophilic and decrease the interaction energy between the graphene layers (the interlayer distance increases from ~0.35 nm in graphite to ~0.7 nm in oxidized graphite).[9,14] Hence, graphite oxide can be readily exfoliated, forming a stable aqueous dispersion. A complete model to describe the exact ratio and spatial distribution of the functional groups that decorate the honeycomb carbon lattice has yet to be elucidated.[15–17]

Graphene oxide is electrically insulating and must be reduced (using chemical and/or thermal treatment) to make it electrically active.[18] Although other methods have been reported,[19] the most

[*] Dr. C. Mattevi, Prof. M. Chhowalla, G. Eda, and Dr. S. Miller
Materials Science and Engineering
Rutgers University, 607 Taylor Road
Piscataway, New Jersey 08854 (USA)
E-mail: cmattevi@rci.rutgers.edu; manish1@rci.rutgers.edu
Dr. S. Agnoli, Prof. G. Granozzi
Department of Chemical Science
University of Padova,
Via Marzolo 1, I-35131 Padova (Italy)
Prof. K. A. Mkhoyan
Department of Chemical Engineering and Materials Science
University of Minnesota
Minneapolis, Minnesota 55455 (USA)
O. Celik, D. Mastrogiovanni, and Prof. E. Garfunkel
Department of Chemistry and Chemical Biology
Rutgers University, 607 Taylor Road
Piscataway, New Jersey 08854 (USA)

DOI: 10.1002/adfm.200900166

widely used chemical route to reduce GO in solution as well as after deposition onto substrates is exposure to hydrazine (as the hydrate, as anhydrous hydrazine, or as dimethylhydrazine vapor).[9,18,20–25] To further improve the electrical properties of reduced GO, the hydrazine treatment is usually followed by thermal annealing (200–500 °C).[10,22] Although these reduction treatments have yielded reasonably good optoelectronic properties, the final electrical transport properties[10,22,26] (such as transconductance in a transistor geometry) are far from those of graphene.[1,27] Obtaining ideal electrical properties of reduced GO has been challenging due to the absence of knowledge regarding the chemical and structural characteristics of reduced GO.

Although various properties of reduced GO have been reported, detailed studies correlating the structure with optical and electrical properties are lacking. Here, we present a comprehensive description of the electronic properties, chemical state, and the structure of uniform GO thin films at different stages of the reduction process. We applied two reduction processes to GO: i) exposure to hydrazine monohydrate vapor and ii) thermal annealing in different environments. We also analyzed the suitability of combined hydrazine and thermal reduction treatments to achieve the desired electrical properties. The present reduction methods utilizing hydrazine and high temperature annealing are not ideal for environmental and technological reasons, respectively. However, understanding the structural and chemical changes that occur during reduction may allow the development of alternative processes.

## 2. Results

In our previous work, deposition of uniform GO thin films with a controllable number of layers from solution at room temperature on a variety of substrates was demonstrated.[10] The vacuum filtration method allows precise control over the number of GO layers so that thin films from a single layer up to 10 layers can be obtained. The reduction process consisting of hydrazine vapor exposure at 80 °C and/or thermal annealing is then applied. This deposition method permits the fabrication of thin film transistors (TFTs) and other devices on a variety of substrates without the use of extensive lithography.[10]

The present study focuses on the reduction process via thermal treatment in UHV and in an $Ar/H_2$ reducing atmosphere on pristine GO thin films and those that have been previously treated with hydrazine vapor. We studied the progressive loss of oxygen functional groups after each step of the reduction process by in situ X-Ray photoelectron spectroscopy (XPS) to reveal the nature of carbon and oxygen bonds. The carbon and oxygen 1 s core level spectra collected on a GO thin film (7 layers) after in situ annealing at temperatures increasing from 100 °C to 450 °C are shown in Figure 1. The carbon and oxygen (inset) 1 s core level spectra for a GO thin film annealed in situ at 650 and 1100 °C are shown in Figure 1c. The high temperature spectra are shown separately because they come from different set of samples. We used quartz substrates for high temperature (650 and 1100 °C) annealing measurements. In addition, slightly higher thickness films (15 ML) were used to ensure the signal collected was free of oxygen signal from the substrate. A thin film of Au (10 nm) was deposited on $SiO_2$ (300 nm)/Si to allow the detection of oxygen from the GO film. The fits used to extract the various C/C and C/O bonding configurations and their concentrations are indicated in the lowermost spectra in Figure 1. The carbon/oxygen ratio was found to be 2.5/1 in pristine GO which is in agreement with values reported for similar oxidation processes.[28,29] Under the experimental conditions used here, the XPS sampling depth is lower for the O 1s signal than for the C 1s by 20% due to the higher binding energy of the O 1s electrons.[30,31] Therefore the O 1s spectra are likely to be slightly more surface specific. This difference becomes more dramatic with increase in the thickness of GO thin films (see for example the difference between a seven-layered and a single-layered GO film).

The C 1s signal of fully oxidized GO consists of five different chemically shifted components which can be deconvoluted into: C=C/C−C in aromatic rings (284.6 eV); C−O (286.1 eV); C=O (287.5 eV); C(=O)-(OH) (289.2 eV); and $\pi$–$\pi^*$ satellite peak (290.6 eV) (Fig. 1a). These assignments are in agreement with previous works.[28,32] We fit the C 1s peak component related to $sp^2$ C−C bonding with Doniach–Sunjic line shape with zero asymmetry due to the absence of C−C $sp^3$ (binding energies in range 285.5–286.5 eV[32]) bonding. This allowed us to monitor the evolution of carbon $sp^2$ bonding with annealing. We found that a maximum carbon $sp^2$ fraction of ~80% can be obtained upon annealing to 1100 °C (see below). The spectra in Figure 1a, b, and c indicate that a large fraction of oxygen atoms form single bonds with the carbon atoms in the basal plane of GO.

The C−O bonds (38.7 at % of carbon atoms in pristine GO) come from epoxy and hydroxyl groups in the basal plane. Based on the XPS results, the GO synthesis method that we utilized (which includes peracid ($KMnO_4$) as

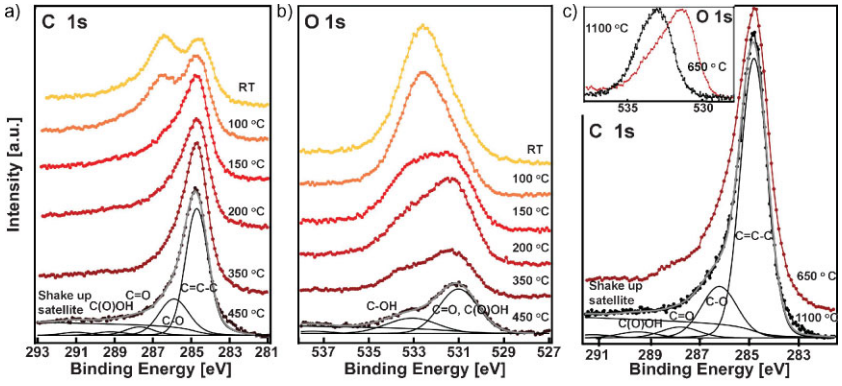


**Figure 1.** a) C1s XPS spectra ($h\nu = 1253.6$ eV) collected on 7 layered GO deposited on Au(10 nm)/$SiO_2$(300 nm)/Si and annealed in UHV at the indicated temperatures for 15 min. The spectra were fit by Doniach-Sunjic function after subtracting a Shirley background as indicated in the lowermost spectrum. The different components related to various chemical shifts of carbon bonds are indicated; b) corresponding O1s XPS spectra c) C1s and related O1s (inset) XPS spectra ($h\nu = 1253.6$ eV) collected on 15 layered GO deposited on quartz and annealed in UHV at the indicated temperatures for 15 min.

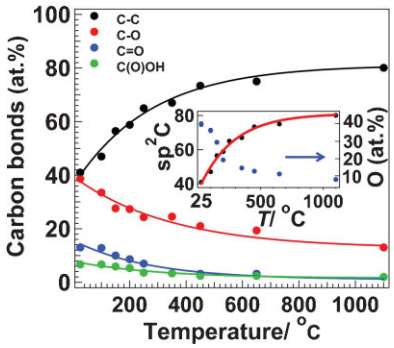


**Figure 2.** The atomic percentages of different carbon bonds identified by XPS as a function of annealing temperature. The $sp^2$ carbon and the corresponding oxygen concentration are reported as a function of the annealing temperature in the inset.

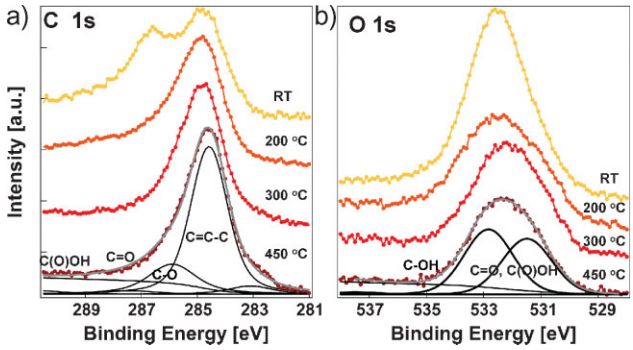


**Figure 3.** a) C 1s XPS spectra ($h\nu = 1253.6$ eV) collected on single-layered GO thin film deposited on Au(10 nm)/$SiO_2$(300 nm)/Si and annealed in UHV at the indicated temperatures for 15 min. The different components related to various chemical shifts of carbon bonds are indicated; b) corresponding O 1s XPS spectra.

the oxidant), and molecular dynamics (MD) simulations,[12,13] we expect that ~20% more epoxy groups are present as compared to hydroxyl groups. Our observations indicate that majority of oxygen species consist of C–O and more oxidized species such as C=O and C=O (O) are present in lesser amounts. The C=O (13 at % in GO) compounds mainly arise from single ketones and quinones[33] which decorate the edges of GO sheets but may also be bound to the basal plane as carbonyl groups.[16,34] The C(O)OH species (6.7 at % in GO) are present primarily at the edges of GO sheets.[15,17,34] Complementary in situ IR measurements suggest the presence of these for functional groups.

The evolution of carbon bonds in GO thin films monitored with XPS as a function of annealing temperature in UHV is summarized in Figure 2. In addition, the evolution of physisorbed species ($H_2O$ and $CO_2$) after 15 min of annealing at 100 °C was confirmed by mass spectroscopy during annealing. The loss of all oxygen groups occurs upon increasing the temperature, exhibiting a higher rate of loss between 100–250 °C (Fig. 2) while C–O component continues to decrease up to 450 °C. The overall rate of oxygen evolution is lower between 300–450 °C in comparison with the loss recorded between 150–300 °C. The C/O atomic ratio at 450 °C is 7.9, in agreement with values reported in the literature for UHV annealing.[29] Initially, the O 1s appears at binding energy of 532.6 eV, in accordance with Ref.[28], because it contains contributions from C=O (531.2 eV), C(=O)-(OH) (531.2 eV) and C–O (533 eV). During annealing, the two components related to C=O and C–O are clearly visible. The fact that we observed C=O peak with higher intensity than the C–O component at annealing temperatures from 200–450 °C could be attributed to the fact that a portion of the O 1s peak incorporates a contribution from trapped $CO_2$ molecules which are present as by-products of the reduction process, as confirmed by in situ IR measurements on thick GO samples.[35] The O 1s peak detected on 1–2 layers GO and annealed between 200–450 °C does not show this additional contribution (see Fig. 3). In addition, the C=O component of the O 1s peak after annealing the single layer films at 1100 °C has lower intensity than the C–O component, as also observed by Yang et al.[29]. Based on the fact that the sampling depth of the O 1s signal is lower than that of C 1s, we tentatively attribute the higher contribution of C=O component with respect to C–O to trapped $CO_2$ in multilayered GO annealed between 150–650 °C.

The fraction of $sp^2$ carbon and the oxygen concentration with annealing temperature are shown in the inset of Figure 2. The concentration of carbon and oxygen are given in atomic percentages (at. %). The at. % for different carbon functional groups is calculated with respect to the total area of the C1s peak. The oxygen at. % is calculated with respect to the total area of the C1s peak plus the O1s peak (taking into account the sensitivity factors). It can be seen that the amount of carbon $sp^2$ bonding increases with loss of oxygen, reaching a maximum value of ~80% at an oxygen content of ~8 at. % (C:O ratio 12.5:1). This suggests that the remaining oxygen is responsible for ~20% $sp^3$ bonding. Thus, annealing up to 1100 °C is not sufficient to completely remove the oxygen from GO.

During the thermal reduction process, GO is expected to undergo structural changes due to the loss of oxygen. The carbon atoms in the basal plane may also rearrange during annealing due to the available thermal energy. Such structural changes were monitored by Raman spectroscopy via measurements taken after each annealing step. The Raman spectra of as prepared and reduced GO thin films consisting of 7 layers are shown in Figure 4. Results from two types of reduction treatments are plotted, annealing at 1100 °C and exposure to hydrazine vapor followed by annealing at 200 °C. The spectra display the carbon D and G band peaks at ~1330 and ~1600 $cm^{-1}$, respectively. The position of the G peak is consistent with that of pristine and hydrazine vapor reduced GO.[22] It is well documented[36–39] that the area ratio of the D and G bands is a measure of the size of $sp^2$ ring clusters in a network of $sp^3$ and $sp^2$ bonded carbon. Using the empirical Tuinstra-Koenig relation[37] to obtain the lateral dimension of $sp^2$ ring clusters, an average graphitic domain size of ~2.5 nm in pristine GO was calculated. After chemical (with hydrazine vapor) reduction and thermal annealing up to 500 °C, the change in the D/G peak area ratio was found to be negligible, in accordance with our previous work.[22] Only after annealing at 1100 °C was a slight decrease in the FWHM of the D peak observed, resulting in an increase in the size of the $sp^2$ cluster to ~2.8 nm (Fig. 4). This observation suggests that even when the $sp^2$ carbon-carbon bonds are restored by de-oxidation, their spatial distribution in the honeycomb graphene lattice does not generate an expansion of a continuous $sp^2$ phase. This may be due to the fact that the $sp^2$ sites

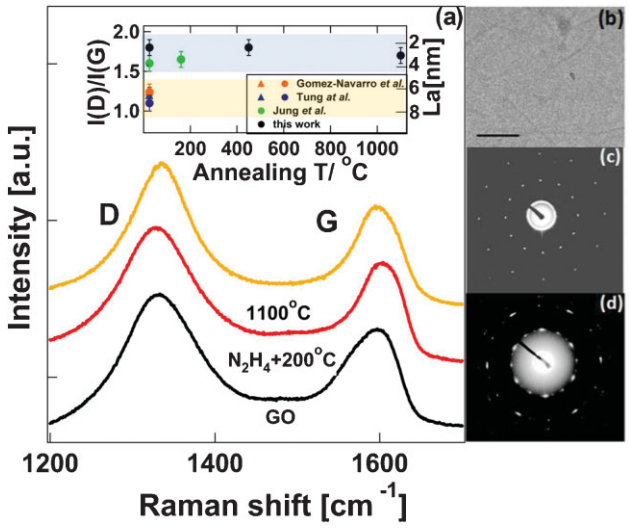


**Figure 4.** a) Raman spectra of 7 layered GO thin films recorded with $\lambda = 633$ nm laser with a lateral beam dimension of ~2 μm. Spectra of pristine GO (black curve), reduced GO via exposure to hydrazine monohydrate vapor at 80 °C followed by annealing at 200 °C (red curve) and GO reduced by annealing only at 1100 °C (yellow curve) are shown. In the inset, the I(D)/I(G) ratio and the related average $sp^2$ cluster sizes of GO thin films before and after reduction reported in the literature along with our results are shown. b) TEM image of few layered chemically reduced reduced GO (Scale bar = 200 nm). Corresponding diffraction patterns are taken from c) pristine GO and d) chemically reduced GO followed by annealing. Both diffraction patterns show the six-fold rotational symmetry expected for diffraction with the beam incident along the [001] direction. The innermost diffraction spots are from (100) planes (d-spacing 0.21 nm) while the outer are from (110) planes (d-spacing 0.12 nm).

are isolated in a way that for every pair of aromatic rings restored as phenol groups, there is also a vacancy in the lattice. In addition, dangling bonds may also be generated from the detachment of CO groups, especially at high temperature (1100 °C). It is well known in graphite that such dangling bonds are difficult to anneal out even at temperatures in excess of 1000 °C.[40,41]

The ratio of the D and G peaks and the corresponding $sp^2$ cluster size with annealing temperature are summarized in the inset of Figure 4. The data from other researchers are also plotted. Our values are in good agreement with the measurements of Jung et al.[42] and Gomez-Navarro et al.[22] but differ from those of Tung et al.[25] who report much lower D to G peaks ratios and therefore much larger $sp^2$ cluster sizes (~6 nm). It should be noted that the electrical properties of the large $sp^2$ cluster size of GO flakes are remarkable, with mobility values ranging from 800–1000 $cm^2 V s^{-1}$.[25] This suggests that large $sp^2$ domain sizes that are minimally interrupted by $sp^3$ bonds due to the presence of oxygen are essential for obtaining exceptional electrical properties in reduced GO. It should be pointed out that the origin of the large $sp^2$ graphitic domain sizes for non-reduced GO in Ref.[25] is unclear but may point to incomplete oxidation of graphite. However, this is not supported by their XPS data from the supplementary information of Ref.[25] in which an oxygen content of ~7–8% is reported, comparable to our results here.

To further examine any remarkable morphological and structural changes between pristine and reduced GO, we also performed selected area diffraction pattern (SAED) using a JEOL 2010F scanning transmission electron microscope (STEM). A TEM image of a few layered GO sheets after reduction by hydrazine monohydrate followed by annealing at 200 °C in vacuum is shown in Figure 4b. The morphology of chemically modified GO appeared quite similar to that of pristine GO, consistent with our previous work.[43] That is, it appears as randomly folded and wrinkled atomic sheets (Fig. 4b). These features are typical of GO[16] but have not been observed in exfoliated graphene.[16] The diffraction patterns of 1–3 layered pristine and reduced (chemically and annealed at 200 °C) GO are shown in Figure 4c and d, respectively. The diffraction patterns taken before and after the reduction revealed that the structure of GO did not change dramatically. Strong diffraction spots with six-fold rotational symmetry are observed in GO, indicating that the electron beam is incident along the [001] direction. Both patterns (Fig. 4c and d) exhibit several sets of diffraction spots arising from folded regions in the sheets (always normal to the incident beam). The innermost diffraction spots are from (100) planes (d-spacing = 0.21 nm) while the outer from (110) planes (d-spacing = 0.12 nm). The fact that GO exhibits diffraction with single spots suggests that the aromatic ring clusters are extended and present in sufficient number to form a pattern typical of crystalline materials. Although the diffraction patterns were not collected on the same flake before and after annealing, the measurements have been repeated over 50 times on different sheets and the results are consistent.

We have correlated the effects of structural changes and the progressive increase in $sp^2$ bonding (and hence the concentration of $\pi$ electrons) on the optoelectronic properties of GO thin films at different stages of reduction treatments. The increase in conductivity of GO thin films as a function of exposure time to hydrazine vapor at 80 °C is shown in Figure 5a. It can be seen that the conductivity reaches a saturation value (10 S $cm^{-1}$) after ~7 h of exposure. The conductivity as a function of the annealing temperature for as-deposited and GO thin films previously exposed to hydrazine monohydrate for 24 hrs are reported in Figure 5b. It can be seen that an increase in conductivity up to ~5.5 $10^2$ S $cm^{-1}$ can be achieved for both cases at 1100 °C. From Figure 5a and b, it is noticeable that the sample pre-treated with hydrazine prior to annealing and straight thermal annealing exhibit comparable values at high temperatures. Figure 5b includes data for both UHV and $Ar/H_2$ annealing, which show that there is little difference in film properties between the two for our case. This is likely due to the fact that careful evacuation and flushing of the annealing chamber was conducted prior to introducing the $Ar/H_2$ mixture and commencing the annealing cycles. The corresponding transmittance values (at $\lambda = 550$ nm) as a function of annealing temperature are shown in Figure 5c and d. It can be seen that chemical reduction and thermal annealing of GO leads to a progressive decrease in transparency of the thin films, reaching a saturation value of ~85%, consistent with an increased concentration of $\pi$ electrons.

Transistors were fabricated on three layered thin films annealed at different reduction treatments to evaluate the evolution of mobility and carrier concentration. We used relatively long channel length (21 μm, $SiO_2$ thickness = 300 nm, channel width = 400 μm) devices to ensure that the transport is bulk

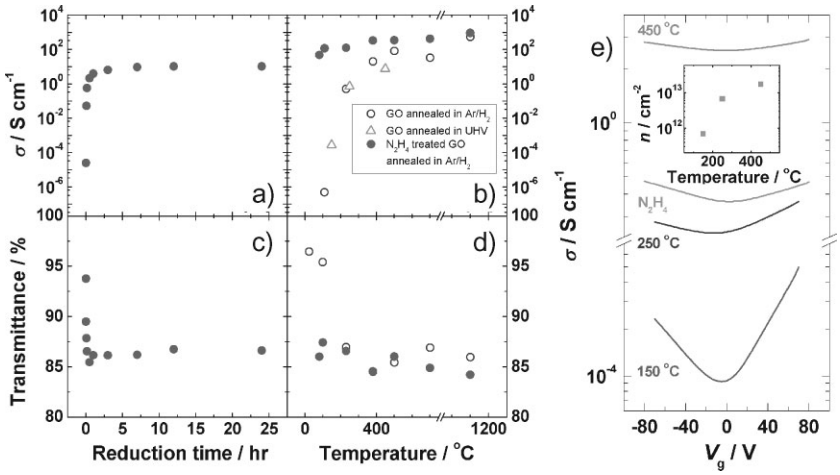


**Figure 5.** Electrical and optical properties of three layered GO: a) conductivity as a function of exposure time to hydrazine monohydrate vapor at 80 °C; b) conductivity of GO exposed for 24 hrs to hydrazine monohydrate vapor at 80 °C and then annealed at increasing temperatures (solid dots), pristine GO annealed in $Ar/H_2$ (open dots) and UHV (triangles); c) transmittance at $\lambda = 550$ nm of GO as a function of exposure time to hydrazine monohydrate vapor at 80 °C; d) Transmittance at $\lambda = 550$ nm of GO film exposed for 24 hrs to hydrazine monohydrate vapor at 80 °C and then annealed at increasing temperatures (solid dots) and pristine GO annealed in $Ar/H_2$ (open dots); e) transfer characteristics of TFT devices based on reduced three layered GO thin films deposited on $SiO_2$(300 nm)/Si for three different annealing temperatures (150, 250, 450 °C) and for reduction via hydrazine. The carrier concentration as function of annealing temperature is reported in the inset. Measurements were conducted in vacuum.

limited and the role of contacts is minimal. The transfer characteristics of films annealed in UHV at three different temperatures (150, 250, 450 °C) and devices on films reduced by hydrazine monohydrate are shown in Figure 5e. The devices exhibit ambipolar characteristics for the measurements performed in vacuum. The main difference among the three devices is that the 'V' shape of the ambipolar graphene transfer characteristics is more pronounced for GO reduced at 150 °C compared to films reduced at 450 °C. That is, the on/off ratio of the film annealed at 150 °C is ~10 which decreases to ~2 with further reduction. The chemically reduced GO also exhibits the 'V' shape, comparable to devices on films annealed at 250 °C. These results demonstrate the semiconducting nature of mildly reduced GO thin films, which become semi-metallic at higher annealing temperatures (as observed in Ref.[10] for thicknesses greater than 1 layer). The corresponding carrier concentration as a function of the annealing temperature is reported in the inset in Figure 5e. The increase in carrier concentration can be attributed to the creation of $\pi$ electrons via chemical reduction. The mobility of the devices in vacuum calculated from the linear regime of the transfer characteristics[10] also increased with reduction level. Specifically, the values increased by five orders of magnitude to ~1 $cm^2 V^{-1} sec^{-1}$ for holes and electrons.

To put the results of this study in context with reports in the literature, we compare our data of transmittance versus sheet resistance with several other studies in Figure 6.[10,23,24,44,45] The plot indicates that the transmittance and sheet resistance decrease with reduction and the overall film thickness. The results clearly demonstrate that the optoelectronic properties of reduced GO reported by various groups are comparable. The stars represent our values for the same film thickness annealed at increasing temperatures. Our reduction via thermal annealing data most closely match with the results of Becerril et al.[24] Furthermore, the hydrazine monohydrate reduction route shows a larger improvement in properties compared to dimethylhydrazine[10] even without subsequent annealing. The results clearly indicate that the reduced GO values reported in the literature do not approach those of intrinsic graphene. Surprisingly, the conductivity and transmittance of graphene from exfoliation of graphite in organic solvents[4] and via heating to 1000 °C[24,45] also do not approach values of intrinsic graphene and are inferior to values of reduced GO.

To elucidate the mechanisms limiting the electronic properties of reduced GO, we investigated the role of residual oxygen and the $sp^2$ bonding fraction. The plot of conductivity as a function of $sp^2$ bonding fraction in reduced GO thin films is shown in Figure 7. Our experimental data along with those from 100% $sp^2$ bonded materials (graphene and graphite) are plotted. Extrapolation of the experimental data suggests that it should be possible to obtain the conductivity of polycrystalline graphite ($1.25 \times 10^3$ S $cm^{-1}$)[45] at an $sp^2$ bonding fraction of ~0.87 in reduced GO. Indeed, recent work by Tung et al.[25] indicates that achieving an $sp^2$ fraction of ~0.85 in conjunction with large $sp^2$ domain sizes (~6 nm from Raman) yields significantly enhanced electrical performance. The con-

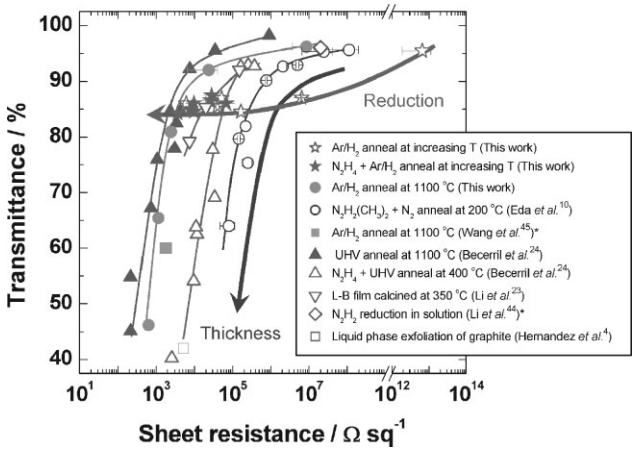


**Figure 6.** Transmittance (at $\lambda = 550$ nm) as a function of sheet resistance of reduced GO thin films from various studies reported in the literature. In some cases, indicated by (*), the properties had to be estimated from the information provided. The stars represent our values for the same film thickness annealed at increasing temperatures. Our data of reduction via thermal annealing concur with the work of Becerril et al. [24] where a similar reduction process was applied. Annealing at 1100 °C in vacuum or in $Ar/H_z$was found to be the most effective reduction route.

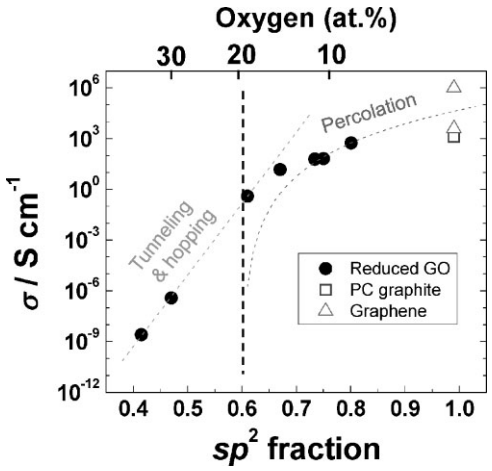


**Figure 7.** Conductivity of thermally reduced GO as a function of the $sp^2$ carbon fraction. The vertical dashed line indicates the percolation threshold at $sp^2$ fraction of ~0.6. Fitting of the experimental data reveals two different regimes for electrical transport with $sp^2$ fraction. Tunneling and/or hopping (straight dashed line) mechanisms dominate at $sp^2$ fractions below 0.6 while percolation amongst the $sp^2$ clusters dominates above the percolation threshold. The 100% $sp^2$ materials are polycrystalline (PC) graphite and graphene. The two conductivity values are for doped by gating (upper triangle) and intrinsic graphene (lower triangle).

ductivity of single-layered graphene ($6 \times 10^3$ S cm$^{-1}$)[27] may be possible by further increasing the $sp^2$ bonding fraction to 0.95. Although the $sp^2$ bonding fraction in the reduced GO reported here is substantial (~0.80), the carrier transport is not only determined by the amount of $\pi$ electrons available but also by their spatial distribution with respect to $sp^3$ sites resulting from residual oxygen.

A structural model that captures the essential features of transport through an individual GO sheet at different stages of reduction is indicated by a series of sketches in Figure 8. The transport in GO thin films is primarily dictated by transport within the sheet and not limited by junctions between the flakes as the mobility values of the thin films are comparable to individual flake values. In Figure 8a, $sp^2$ clusters isolated by oxygen atoms (indicated by light gray dots) are shown. As the material is progressively reduced, interactions (hopping and tunneling) among the clusters increase (Fig. 8b). Further reduction by removal of oxygen leads to greater connectivity among the original graphitic domains by formation of new smaller $sp^2$ clusters, in addition to an increase in structural defects via evolution of CO and/or $CO_2$ species (especially from epoxy groups), indicated as pentagons in Figure 8c and d. Thus, transport in the initial stages of reduction occurs via tunneling or hopping among the $sp^2$ clusters, as indicated by the exponential fit of the data in Figure 7 at low $sp^2$ fractions. At higher $sp^2$ concentrations, percolation ($\sigma = A(x - x_c)^{\alpha}$) amongst the $sp^2$ clusters of various shapes and sizes dominates the transport as indicated by the curve fit in Figure 7. The percolation threshold was found experimentally to occur at an $sp^2$ concentration of 60% which is in agreement with theoretical threshold values for conduction among two dimensional disks.[46] The critical exponent ($\alpha$) was found to be 6.53. It is well known from percolation theory that critical exponents greater than three are a consequence of strictly geometrical effects (such as thin resistive bottlenecks) and tunneling effects.[47,48] Both cases are applicable to reduced GO where percolation amongst the $sp^2$ clusters is mitigated by structural defects or resistive bottlenecks formed by limited conduction paths due to the presence of residual oxygen.

We have investigated the evolution of graphene oxide (GO) as a function of reduction treatment and demonstrated that annealing at 450 °C or above is equivalent to chemical reduction via hydrazine monohydrate at 80 °C followed by heating at 200 °C. Chemical characterization by XPS shows dramatic changes in the chemical state of the material with temperature. For fully reduced GO, we found the oxygen content to be ~8% (C:O ratio12.5:1) with the $sp^2$ concentration being 80%. The structural changes monitored by Raman to probe the $sp^2$ graphitic domain sizes revealed little or no increase below 1100 °C. STEM observations confirmed the Raman structural results. By monitoring the conductivity versus the $sp^2$ fraction, we demonstrate that the presence of residual oxygen (~8 at. %) significantly hampers the carrier transport among the graphitic domains. Fitting the experimental data reveals that transport at the initial stages of reduction is dominated by hopping or tunneling amongst the $sp^2$ clusters. At latter stages of reduction the original $sp^2$ clusters are connected by newly formed smaller $sp^2$ domains so that transport by percolation can occur. However, carrier transport above the percolation threshold is limited by conduction bottlenecks amongst the clusters. A detailed study of transport will be reported elsewhere.

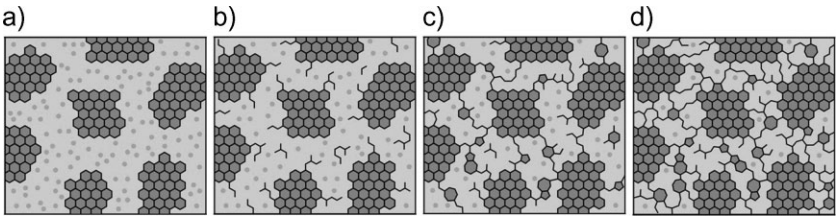


**Figure 8.** Structural model of GO at different stages of reduction by thermal annealing at: a) room temperature; b) ~100 °C; c) ~220 °C; d) ~500 °C. The dark gray areas represent $sp^2$ carbon clusters and the light gray areas represents $sp^3$ carbon bonded to oxygen groups (represented by small dots). At ~220 °C, the percolation among the $sp^2$ clusters initiates (corresponding to $sp^2$ fraction of ~0.6).

## Acknowledgements

We thank F. Cosandey for assistance with STEM analysis and financial support from the NSF CAREER Award (ECS 0543867).

Received: January 21, 2009
Revised: March 9, 2009
Published online:

[1] K. S. Novoselov, A. K. Geim, S. V. Morozov, D. Jiang, M. I. Katsnelson, I. V. Grigorieva, S. V. Dubonos, A. A. Firsov, *Nature* **2005**, *438*, 197.

[2] Y. Zhang, Y.-W. Tan, H. L. Stormer, P. Kim, *Nature* **2005**, *438*, 201.
[3] K. S. Novoselov, D. Jiang, F. Schedin, T. J. Booth, V. V. Khotkevich, S. V. Morozov, A. K. Geim, *Proc. Natl. Acad. Sci. U. S. A.* **2004**, *102*, 10453.
[4] Y. Hernandez, V. Nicolosi, M. Lotya, F. M. Blighe, Z. Sun, S. De, I. T. McGovern, B. Holland, M. Byrne, Y. K. Gun'kp, J. J. Boland, P. Niraj, G. Duesberg, S. Krishnamurthy, R. Goodhue, J. Hutchison, V. Scardaci, A. C. Ferrari, J. N. Coleman, *Nat. Nanotechnol.* **2008**, *3*, 563.
[5] S. Y. Zhou, G. H. Gweo, A. V. Fedorov, P. N. First, W. A. D. Heer, D. H. Lee, F. Guinea, A. H. C. Neto, A. Lanzara, *Nat. Mater.* **2007**, *6*, 770.
[6] C. Berger, Z. Song, X. Li, X. Wu, N. Brown, C. Naud, D. Mayou, T. Li, J. Hass, A. N. Marchenkov, E. H. Conrad, P. N. First, W. A. de Heer, *Science* **2006**, *312*, 1191.
[7] S. Marchini, S. Gunther, J. Wintterlin, *Phys. Rev. B* **2007**, *76*, 075429.
[8] A. Reina, X. Jia, J. Ho, D. Nezich, H. Son, V. Bulovic, M. S. Dresselhaus, J. Kong, *Nano Lett.* **2009**, *9*, 35.
[9] S. Stankovich, D. A. Dikin, R. D. Piner, K. A. Kohlhaas, A. Kleinhammes, Y. Jia, Y. Wu, S. T. Nguyen, R. S. Ruoff, *Carbon* **2007**, *45*, 1558.
[10] G. Eda, G. Fanchini, M. Chhowalla, *Nat. Nanotechnol.* **2008**, *3*, 270.
[11] X. Liang, Z. Fu, S. Y. Chou, *Nano Lett.* **2007**, *7*, 3840.
[12] J. T. Paci, T. Belytschko, G. C. Schatz, *J. Phys. Chem. C* **2007**, *222*, 18099.
[13] J. Chattopadhyay, A. Mukherjee, C. E. Hamilton, J. Kang, S. Chakraborty, W. Guo, K. F. Kelly, A. R. Barron, W. E. Billups, *J. Am. Chem. Soc.* **2008**, *130*, 5414.
[14] D. W. Boukhvalov, M. I. Katsnelson, *J. Am. Chem. Soc.* **2008**, *130*, 10697.
[15] A. Lerf, H. He, M. Forster, J. Klinowski, *J. Phys. Chem. B* **1998**, *102*, 4477.
[16] T. Szabó, O. Berkesi, P. Forgó, K. Josepovits, Y. Sanakis, D. Petridis, I. Dékány, *Chem. Mater.* **2006**, *18*, 2740.
[17] H. He, J. Klinowski, M. Forster, A. Lerf, *Chem. Phys. Lett.* **1998**, *287*, 53.
[18] S. Stankovich, D. A. Dikin, G. H. B. Dommett, K. M. Kohlhaas, E. J. Zimney, E. A. Stach, R. D. Piner, S. T. Nguyen, R. S. Ruoff, *Nature* **2006**, *442*, 282.
[19] Y. Si, E. T. Samulski, *Nano Lett.* **2008**, *8*, 1679.
[20] S. Gilje, S. Han, M. Wang, K. L. Wang, R. B. Kaner, *Nano Lett.* **2007**, *7*, 3394.
[21] J. T. Robinson, M. Zalalutdinov, J. W. Baldwin, E. S. Snow, Z. Wei, P. Sheehan, B. H. Houston, *Nano Lett.* **2008**, *8*, 3441.
[22] C. Gomez-Navarro, R. T. Weitz, A. M. Bittner, M. Scolari, A. Mews, M. Burghard, K. Kern, *Nano Lett.* **2007**, *7*, 3499.
[23] X. Li, G. Zhang, X. Bai, X. Sun, X. Wang, E. Wang, H. Dai, *Nat. Nanotechnol.* **2008**, *3*, 538. Correction published on April 23, 2009, DOI: 10.1021/nl901209z
[24] H. A. Becerril, J. Mao, Z. Liu, R. M. Stoltenberg, Z. Bao, Y. Chen, *ACS Nano* **2008**, *2*, 463.
[25] V. C. Tung, M. J. Allen, Y. Yang, R. B. Kaner, *Nat. Nanotechnol.* **2008**, *4*, 25.
[26] S. Wang, P. J. Chia, L. L. Chua, L. H. Zhao, R. Q. Png, S. Sivaramakrishnan, M. Zhou, R. G. S. Goh, R. H. Friend, A. T. S. Wee, P. K. H. Ho, *Adv. Mater.* **2008**, *9999*, 1.
[27] X. Du, I. Skachko, A. Barker, E. Y. Andrei, *Nat. Nanotechnol.* **2008**, *3*, 491.
[28] C. Hontoria-Lucas, A. J. L. Peinando, J. D. D. Lopez-Gonzalez, M. L. Rojas-Cervantes, R. M. Martin-Aranda, *Carbon* **1995**, *33*, 1585.
[29] D. Yang, A. Velamakanni, Gl. Bozoklu, S. Park, M. Stoller, R. D. Piner, S. Stankovich, I. Jung, D. A. Field, C. A. Ventrice Jr., R. S. Ruoff, *Carbon* **2008**, *47*, 145.
[30] QUASES-Tougaard Inc. http://www.quases.com/frames/samples_and_downloads.htmwe (accessed May 2009).
[31] S. Tanuma, C. J. Powell, D. R. Penn, *Surf. Interf. Anal.* **1993**, *21*, 165.
[32] D.-Q. Yang, E. Sacher, *Langmuir* **2006**, *22*, 860.
[33] T. Szabó, O. Berkesi, I. Dékány, *Carbon* **2005**, *43*, 3181.
[34] W. Cai, R. D. Piner, F. J. Stadermann, S. Park, M. A. Shaibat, Y. Ishii, D. Yang, A. Velamakanni, S. J. An, M. Stoller, J. An, D. Chen, R. S. Ruoff, *Science* **2008**, *321*, 1815.
[35] L. Goux, R. Guzman, J.-F. Veyan, Y. J. Chabal, Studies of Graphene Oxidation and Graphene Oxide Reduction by In situ FTIR, presented at AVS 55th International Symposium **2008**, October 19–24 Boston (MA).
[36] A. C. Ferrari, J. Robertson, *Philos. Trans. R. Soc. Lond. Ser. A-Math. Phys. Eng. Sci.* **2004**, *362*, 2477.
[37] F. Tuinstra, J. L. Koenig, *J. Chem. Phys.* **1970**, *53*, 1126.
[38] M. A. Pimenta, G. Dresselhaus, M. S. Dresselhaus, L. G. Cancado, A. Jorio, R. Saito, *Phys. Chem. Chem. Phys.* **2007**, *9,* 1276.
[39] M. Chhowalla, A. C. Ferrari, J. Robertson, G. A. J. Amaratunga, *App. Phys. Lett.* **2000**, *76*, 1419.
[40] F. Banhart, *Rep. Prog. Phys* **1999**, *62*, 1181.
[41] S. R. S. Soares, N. M. Balzaretti, R. P. Livi, A. S. Pereira, J. A. H. d. Jordana, *Nucl. Instrum. Meth. in Phys. Res. B* **2001**, *175*, 474.
[42] I. Jung, D. A. Dikin, R. D. Piner, R. S. Ruoff, *Nano Lett.* **2008**, *8*, 4283.
[43] K. A. Mkhoyan, A. W. Contryman, J. Silcox, D. A. Stewart, G. Eda, C. Mattevi, S. Miller, M. Chhowalla, *Nano Lett.* **2009**, *9*, 1058.
[44] D. Li, M. B. Muller, S. Gilje, R. B. Kaner, G. G. Wallace, *Nat. Nanotechnol.* **2008**, *3*, 101.
[45] X. Wang, L. Zhi, K. Mullen, *Nano Lett.* **2008**, *8*, 324.
[46] G. E. Pike, C. Seager, *Phys. Rev. B* **1974**, *10*, 1421.
[47] D. S. Mclachlan, C. Chiteme, C. Park, K. E. Wise, S. E. Lowther, P. T. Lillehei, E. J. Siochi, J. S. Harrison, *J. Polym. Sci.: Part B: Polym. Phys.* **2005**, *43*, 3273.
[48] I. Balberg, *Phys. Rev. B* **1998**, *57*, 13351.